

Preparation and characterization of Co–BaTiO₃ nano-composite films by the pulsed laser deposition

Wu Weidong^{a,b,*}, He Yingjie^{a,b}, Wang Feng^{a,b}, Chen Zhenghao^{b,c}, Tang Yongjian^b, Sun Weiguo^a

^a*Institute of Physics, Sichuan University, Chengdu, 621900, Sichuan, People's Republic of China*

^b*Research Center of Laser Fusion, Mianyang, 621900, Sichuan, People's Republic of China*

^c*Laboratory of Optical Physics, Institute of Physics and Center for Condensed Matter Physics, Chinese Academy of Sciences, P.O. Box 603, Beijing 100080, People's Republic of China*

Received 29 July 2005; received in revised form 28 October 2005; accepted 8 November 2005

Available online 5 January 2006

Communicated by K. Nakajima

Abstract

The Co–BaTiO₃ nanocomposite films on the MgO (1 0 0) surface were grown with a thickness of about 30–100 nm by using the pulsed laser deposition (PLD) method. Co nanoparticles with the diameter of 5–18 nm were embedded uniformly in the BaTiO₃ matrix. The measurements with the X-ray diffraction (XRD) and high-resolution transmission electron microscopy (HRTEM) indicate that the BaTiO₃ matrix is grown in the (0 0 1) direction with respect to the MgO(1 0 0) surface. The AFM images show that the root of mean squared (RMS) roughness of Co–BaTiO₃ ranges from 0.11 to 0.9 nm. The Raman scattering on the Co–BaTiO₃ nano-composite films shows an enhanced intensity and a shifted wavenumber compared to the pure BaTiO₃ crystal.

© 2005 Elsevier B.V. All rights reserved.

Keywords: A3. Pulsed laser deposition; B1. BaTiO₃; B1. Nanocomposite films

1. Introduction

As a ferroelectric material, the barium titanate (BaTiO₃) film has currently been one of the most technologically and scientifically interesting materials due to its large ferroelectric response, high electro-optic coefficient, second- and third-order nonlinear susceptibility. These properties of BaTiO₃ films can be dramatically improved when metal nanoparticles are embedded in them [1,2]. As known, a large third-order optical nonlinearity is very useful for optical switching devices. However, the enhancement of the third-order nonlinear susceptibility $\chi^{(3)}$ is always accompanied by an increase in the absorption coefficient α . Recent studies [3–6] demonstrate that the third-order nonlinearity of the metal–BaTiO₃ composite film could

be enhanced while the resonant absorption was quenched by embedding structurally anisotropic metal nanoparticles in the BaTiO₃ films. Therefore, it is critical to fabricate the high-quality metal nanoparticles–BaTiO₃ composite film.

At present, the nano-scale cobalt (Co) particles embedded uniformly in BaTiO₃ matrix (Co–BaTiO₃) are prepared using a pulsed laser deposition (PLD) technique. Their structure and morphology were characterized by the X-ray diffraction (XRD), high-resolution transmission electron microscopy (HRTEM) and atomic force microscopy (AFM). The vibration modes were examined by the Raman scattering technique. The results show that the Co–BaTiO₃ films are single crystalline with ultra smooth surfaces.

2. Experiments

The Co–BaTiO₃ films were prepared by using a PLD technique. The experimental parameters are listed in Table 1.

*Corresponding author. Research Center of Laser Fusion, Mianyang, 621900, Sichuan, People's Republic of China. Tel.: 086 816 2484226; fax: 086 816 2493148.

E-mail address: wuweidongding@163.com (W. Weidong).

Table 1
The experimental parameters for the Co–BaTiO₃ films preparation

Back ground vacuum	$\sim 1 \times 10^{-5}$ Pa
Working vacuum	$\sim 1 \times 10^{-4}$ Pa
Substrate temperature	~ 650 °C
Annealing temperature	650 °C/5 Pa O ₂ pressure, 30 min
Target	BaTiO ₃ > 99.9% purity and Co > 99.9% purity
Substrate	MgO(100)
Typical energy density	1.5–2 J/cm ²
Laser pulse frequency	2 Hz for BaTiO ₃ deposition and 4 Hz for Co deposition

Table 2
Characteristics of the Co–BaTiO₃ films

Sample no	Thickness (nm)	The number of laser pulses onto the Co target
1	~100	0
2	~100	20
3	~100	40
4	~100	60
5	~100	80
6	~30	50

During the whole process of deposition, both BaTiO₃ and Co targets were mounted on a rotating holder, alternatively ablated by the pulsed laser beam and deposited onto the MgO(100) substrates. The Co concentration in the films was controlled by adjusting the number of laser pulses focused onto the Co target. The characteristics of Co–BaTiO₃ films are shown in Table 2.

3. Results and discussion

The HRTEM images of sample 6 are shown in Fig. 1. The dark areas in Fig. 1a correspond to Co nanoparticles, whereas the background corresponds to the BaTiO₃ matrix. The diameter of Co nanoparticles in the layer was estimated to be 5–18 nm and the average diameter is about 9 nm. From Fig. 1a, we can observe an approximately homogenous distribution of Co nanoparticles in the BaTiO₃ matrix and their anisotropic geometric outline taking on polygon. Fig. 1b shows that the observed Co nanoparticles contain periodically bright and dark fringes. According to these fringes, the Co nanoparticles are determined to be endowed with a face-center cubic (fcc) structure. In the following, we will present the evidence of the Co nanoparticles with a hexagonal-close-packed (hcp) structure.

The perfect electron-diffraction patterns are shown in Fig. 2 [(a) for 6, (b) for 3]. They are the typical plane and vertical cross-section electron diffraction patterns of the studied samples. The patterns imply that the BaTiO₃

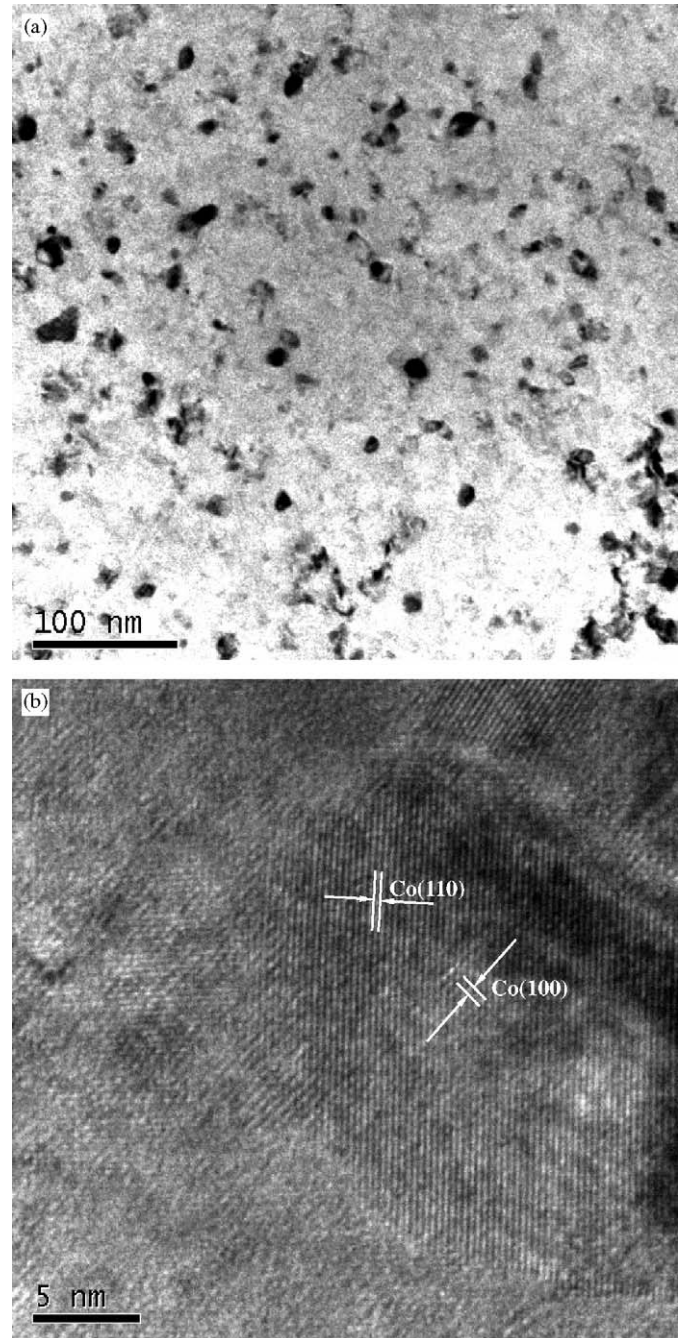


Fig. 1. The HRTEM images of sample 6: (a). overview of Co nanoparticles embedded in the BTO matrix; (b) the HRTEM micrograph of Co nano-particle in sample 6.

matrix is a single phase. As a matter of fact, the bulk BaTiO₃ is weakly tetragonal with the lattice parameters of $a = 0.399$ nm and $c = 0.403$ nm at room temperature. The BaTiO₃ matrix grown on the MgO (100) substrate may be tetragonal or cubic. According to Fig. 2a, we can only calculate $a = 0.410$ nm, and cannot determine the growth direction of the film and whether the sample 6 is tetragonal or not. On the other hand, Fig. 2b indicates $a = 0.424$ nm and $c = 0.407$ nm, a bit larger than the bulk ones due to the

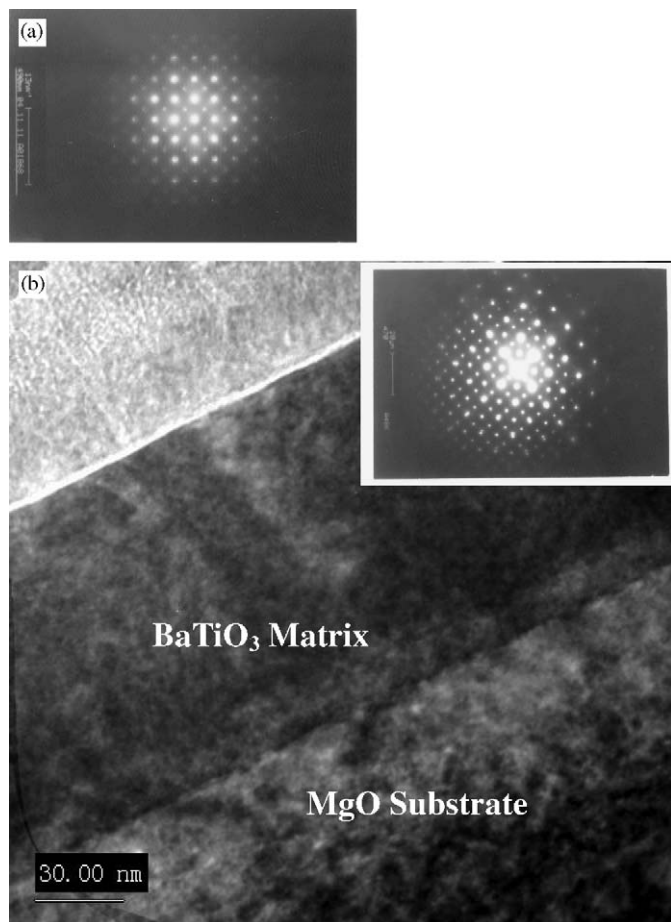


Fig. 2. The electronic pattern of Co–BaTiO₃ HRTEM: (a) the pattern of sample 6 HRTEM; (b) the pattern of sample 3 HRTEM.

lattice match with the MgO (100) surface. The BaTiO₃ matrix of sample 3 is thus deduced to be tetragonal.

The microstructure of the Co–BaTiO₃ composite films grown on the MgO (100) surface was further studied by XRD, as shown in Fig. 3. There are three typical diffraction peaks, of which two are corresponding to BTO-(001)(or BTO-(100))and BTO-(002)(or BTO-(200)) faces of the BaTiO₃ matrix, respectively. According to Fig. 3a, $c \sim 4.08$ for sample 6 and $c \sim 4.07$ for sample 3 agrees with that from Fig. 2b. Based on Figs. 2 and 3, we deduced that the BTO matrix is single tetragonal phase and c -axis perpendicular to (100) MgO substrate. Thus the two peaks of BTO matrix in Fig. 3 correspond to BTO-(001) and BTO-(002), respectively. Further studies show that there are some weak peaks in Fig. 3b corresponding to (100)-hcp Co nanoparticles. The coexistence of the fcc and hcp structure of Co nanoparticles embedded in the BaTiO₃ matrix may result from a small difference of the Gibbs free energy between the two phases of Co crystals.

The mosaicity of the BTO matrix was evaluated by measuring the rocking curve. As shown in Fig. 3c, the full-widths at half-maximum (FWHM) are 1.39° and 1.68° for samples 1 and 3, respectively. This broaden FWHM is

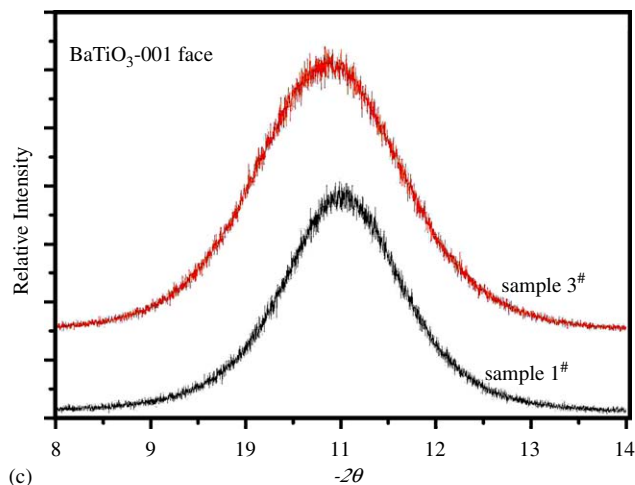
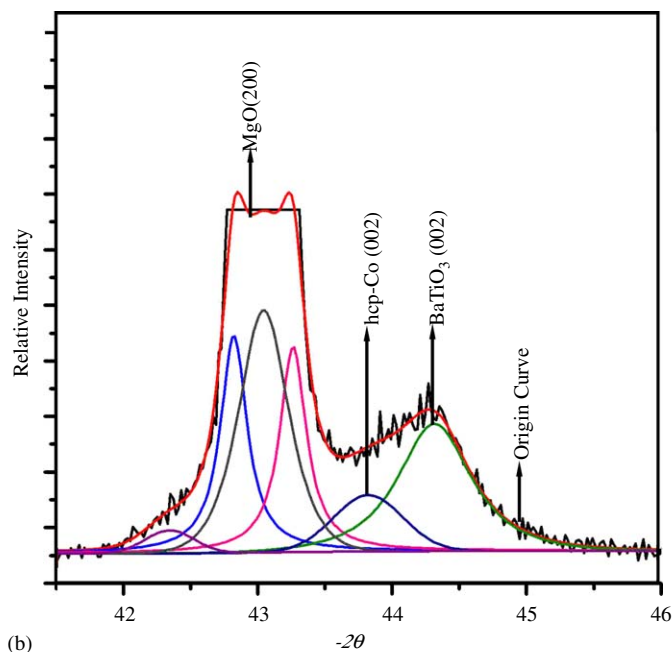
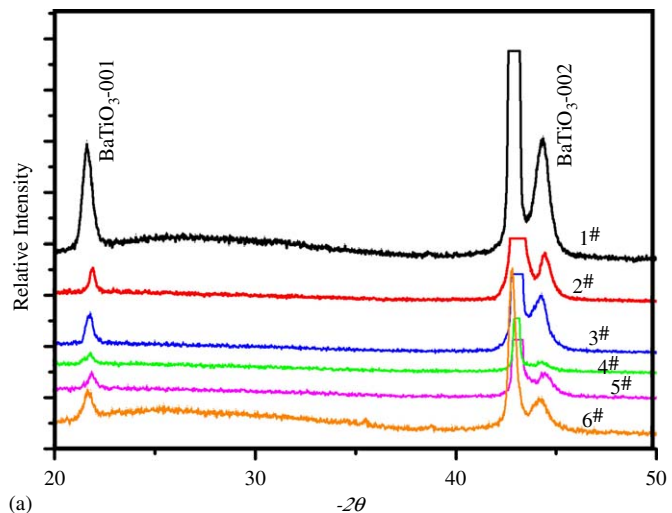


Fig. 3. The XRD spectra of Co–BaTiO₃: (a) the XRD spectra of Co–BaTiO₃ films; (b) the peak fit of sample 3; (c) the rocking curve measurement of sample 1 and 3.

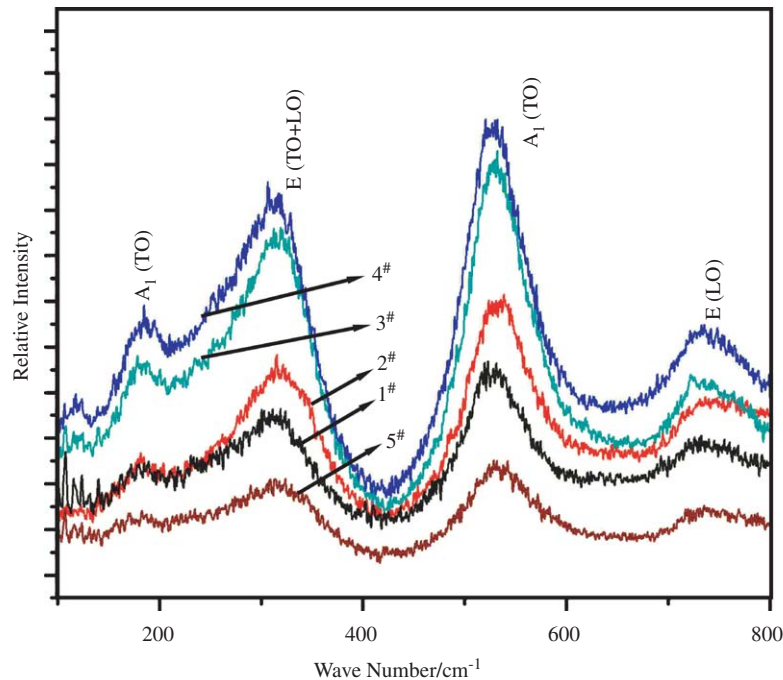


Fig. 4. The Raman spectra of sample 1–5.

Table 3

Wavenumber (in cm^{-1}) of the observed Raman lines for the Co–BaTiO₃ composite film with the tetragonal phase

	Sample no					Mode
	1	2	3	4	5	
Wavenumber (cm^{-1})	179.7	180.3	179.8	182.0	178.0	A ₁ (TO)
	317.6	320.9	320.6	319.1	316.6	E (TO+LO)
	527.1	532.1	529.3	527.0	531.0	A ₁ (TO)
	732.6	739.6	738	737.8	735.2	E (LO)

attributed mainly to the large lattice mismatch between the MgO substrate and the BaTiO₃ matrix.

The BaTiO₃ matrix with the tetragonal phase belongs to the C_{4v} (P_{4mm}) point group, in which the optical vibration modes A and E are both Raman and infrared active and the mode B is only Raman active. The Raman spectra of Co–BaTiO₃ composite films are shown in Fig. 4 and their peak positions are given in Table 3. The lattice distortion and large internal stress in the BaTiO₃ matrix result in Raman shift. The coupling of elemental excitations in the BaTiO₃ matrix with the surface plasmon of the Co nanoparticles enhances the Raman scattering intensity in comparison with the pure BaTiO₃ film.

Figs. 5a–c show the typical AFM images of samples 1, 5 and 6. It indicates that the RMS roughnesses of the Co–BaTiO₃ composite films grown on MgO (100) surface are quite small. The RMS roughnesses are equal to 0.11, 0.32 and 0.14 nm for samples 1, 5 and 6, respectively. In Fig. 5b, the bright hills may represent the Co nanoparticles, indicating that the distribution of the Co nano-particles in

the BaTiO₃ matrix is approximately uniform. The shape of Co nano-particles in Fig. 5b is approximately ellipsoidal and arranged in order.

4. Conclusion

In summary, the single tetragonal-phase Co–BaTiO₃ composite films have been prepared by the PLD method. The Co–BaTiO₃ composite films are epitaxial with respect to the MgO (100) surface. The *c*-axis of these films is perpendicular to the MgO (100) surface. The lattice parameter $a = 4.10$, $c = 4.08$ and $a = 4.24$, $c = 4.07$ for samples 6 and 3, respectively. The AFM images show that the RMS roughnesses of the grown composite films are quite small and equal to 0.11, 0.32 and 0.14 nm for sample 1, 5 and 6, respectively. The interaction between the BaTiO₃ matrix and the Co nanoparticles results in the Raman shift and the enhanced Raman scattering intensity. All the results imply that the Co–BaTiO₃ films could exhibit useful optical properties.

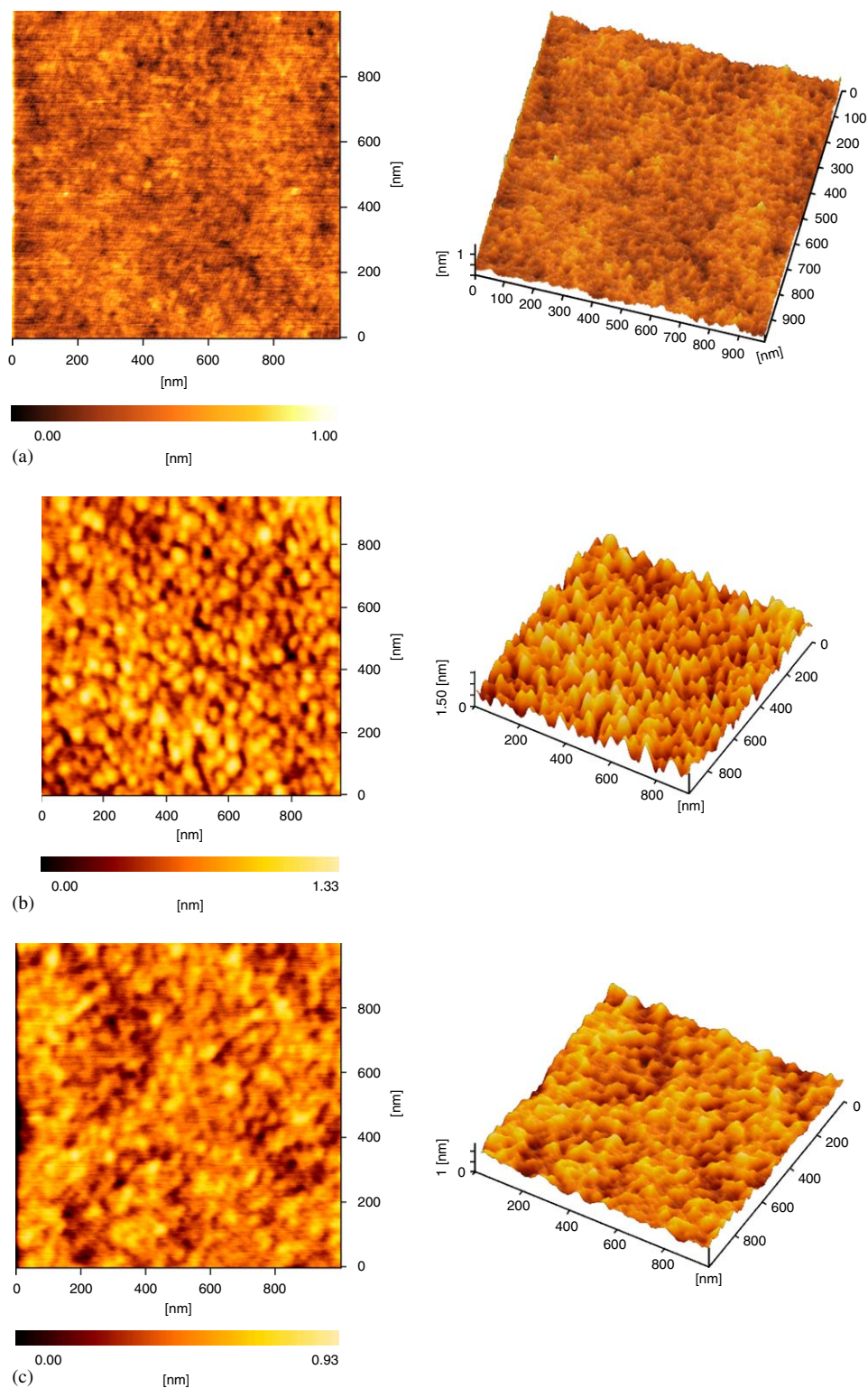


Fig. 5. The typical AFM image of Co-BaTiO₃ films: (a) the AFM image of sample 1; (b) the AFM image of sample 5; (c) the AFM image of sample 6.

Acknowledgements

This work was supported by the National Natural Science Foundation of China, Grant No. 10276037, and Institute

Science Foundation of Research Center of Laser Fusion, Grant No. 9112. The authors would like to thank X. F. Duan for the HRTEM measurements, and also Dr. H. L. Lei and Prof. X. Ju for giving us a very useful discussion.

References

- [1] G. Yang, W.T. Wang, Y.L. Zhou, H.B. Lu, G.Z. Yang, Z.H. Cheng, *Appl. Phys. Lett.* 81 (2002) 3969.
- [2] W.H. Siu, K.W. Yu, *Phys. Rev. B* 53 (1996) 9277.
- [3] K.P. Yuan, M.F. Law, K.W. Yu, P. Sheng, *Opt. Commun.* 148 (1998) 197.
- [4] K.P. Yuan, M.F. Law, K.W. Yu, P. Sheng, *Phys. Rev.* 56 (1997) R1322.
- [5] W.T. Wang, Z.H. Chen, G. Yang, D.Y. Yang, Y.L. Zhou, *Appl. Phys. Lett.* 83 (2003) 1983.
- [6] W.T. Wang, G. Yang, W.D. Wu, Z.H. Chen, *J. Appl. Phys.* 94 (2003) 6837.